INTERNATIONAL JOURNAL FOR NUMERICAL METHODS IN FLUIDS, VOL. 23, 1275–1287 (1996)

EFFECT OF SPANWISE SYSTEM ROTATION ON SPATIALLY DEVELOPING DEAN VORTICES

THÉO RANDRIARIFARA AND ALESSANDRO BOTTARO

IMHEF–DGM, École Polytechnique Fédérale de Lausanne, CH-1015, Lausanne, Switzerland

SUMMARY

Three-dimensional spatially developing Navier–Stokes calculations are carried out to simulate the flow in a curved, rotating channel. The competition between centrifugal and Coriolis forces, expressed by the ratio of the Dean number to the rotation number, gives rise to a variety of possible instability modes characterized by the presence of streamwise vortices. Cases in which the force produced by system rotation enhances or opposes the centrifugal force are treated and the effect on the ensuing instability are analysed. Evidence for a generalized Eckhaus instability of rotating Dean vortices is presented.

KEY WORDS: Dean vortices; system rotation; Eckhaus instability; centrifugal and Coriolis forces

1. INTRODUCTION

Problems of flow with streamline curvature and/or system rotation have attracted much attention in recent years for a number of reasons. These kinds of flows are commonly encountered in several technical applications, e.g. rotating turbomachinery, and understanding the process by which they break down to turbulence might lead to improved models of the flow behaviour on the pressure and suction sides of a blade. One could also envisage ways to affect the near-wall structure of the motions to improve the performance of the machine. Another interesting characteristic of flows with multiple body forces is the possible cancellation of effects when the destabilizing forces oppose each other in such a way as to annihilate instability waves.

The present work is concerned with the spatial development of the flow in a curved channel subject to spanwise system rotation. The motion in a curved channel is susceptible to an instability when the destabilizing centrifugal force exceeds the restoring normal pressure gradient. Under such a condition, steady streamwise 'Dean' vortices[1] ensue. These vortical structures are initially amplified exponentially along x, the streamwise direction, by the instability mechanism; downstream, non-linear effects become important and the vortices reach a saturated stage of (approximately) constant perturbation energy. Details of these phenomena are provided by the experiments of Matsson and Alfredsson[2,3] and Ligrani *et al.*[4] Navier–Stokes simulation results were reported by Finlay *et al.*[5] using a *temporal model* and by Bottaro[6] with a *spatial model*. A feature of these vortices, observed in both experiments and simulations, is their tendency to interact through the merging of neighbouring pairs and/or the appearance of new vortices in between existing pairs. Such events, termed *mergings* and *splittings*, have been studied by Guo and Finlay,[7,8] who explained them in terms of an Eckhaus instability.

CCC 0271–2091/96/121275–13

Received August 1995
Revised January 1996

When spanwise system rotation is applied, a Coriolis force appears which can oppose or enhance the effect of the centrifugal force. Linear theory has been used by Matsson and Alfredsson[9] and Matsson[10] to describe the interaction of these forces during the initial spatial development of the flow in a curved, rotating channel. Matsson and Alfredsson[3] also conducted experiments and demonstrated that moderate negative* rotation can cancel the vortices and strong negative rotation can produce vortices with upwash (secondary flow away from the surface) on the convex wall of the channel (simply put, the vortices are 'upside-down'). This can be qualitatively explained on the basis of an *inviscid* stability criterion, a generalization of the Rayleigh criterion proposed by Mutabazi *et al.*[11] The modified Rayleigh discriminant in the presence of curvature and system rotation is defined by

$$\Phi(r) = 2\frac{u(r)}{r}\left(\frac{\mathrm{d}u(r)}{\mathrm{d}r} + \frac{u(r)}{r}\right) + 6\frac{\Omega u(r)}{r} + 2\Omega\left(\frac{\mathrm{d}u(r)}{\mathrm{d}r} + 2\Omega\right), \tag{1}$$

where $u(r)$ is the base flow velocity distribution, Ω is the angular velocity of rotation and r is the radial co-ordinate. Φ measures the kinetic momentum stratification of fluid particles. A necessary and sufficient condition for inviscid stability to axisymmetric perturbations is $\Phi(r) \geqslant 0$ everywhere in the flow held.

A problem somewhat related to the present one is that of the spanwise rotating boundary layer flow. It was shown by Aouidef *et al.*,[12] Zebib and Bottaro[13] and Bottaro *et al.*[14] via linear and non-linear theories that negative system rotation delays the appearance of the Görtler vortices to downstream distances very far away from the leading edge of the plate. There are no 'upside-down' vortices in this case because of the absence of a convex wall.

The present work treats numerically the problem of the influence of spanwise system rotation on spatially developing Dean vortices. The results illustrate nicely the vortex annihilation effect discussed previously for moderate negative rotation, the 'upside-down' effect for larger negative rotation and the enhancement of the instability produced by position rotation of the system. Furthermore, evidence of an Eckhaus instability for rotating Dean vortices is also presented. Comparisons with the experimental data of Matsson and Alfredsson[2,3] are made throughout.

2. FORMULATION

The development of steady vortices is computed by solving the three-dimensional, incompressible Navier–Stokes and continuity equations expressed in cylindrical co-ordinates (r, θ, z) in the rotating frame of reference sketched in Figure 1:

$$\frac{\mathrm{D}u_r}{\mathrm{D}t} - \frac{u_\theta^2}{r} = -\frac{\partial p}{\partial r} + \frac{1}{Re}\left(\nabla^2 u_r - \frac{u_r}{r^2} - \frac{2}{r^2}\frac{\partial u_\theta}{\partial \theta}\right) + 2Rou_\theta, \tag{2}$$

$$\frac{\mathrm{D}u_\theta}{\mathrm{D}t} + \frac{u_\theta u_r}{r} = -\frac{1}{r}\frac{\partial p}{\partial \theta} + \frac{1}{Re}\left(\nabla^2 u_\theta - \frac{u_\theta}{r^2} + \frac{2}{r^2}\frac{\partial u_r}{\partial \theta}\right) - 2Rou_r, \tag{3}$$

$$\frac{\mathrm{D}u_z}{\mathrm{D}t} = -\frac{\partial p}{\partial z} + \frac{1}{Re}\nabla^2 u_z, \tag{4}$$

$$\frac{1}{r}\frac{\partial u_\theta}{\partial \theta} + \frac{1}{r}\frac{\partial (ru_r)}{\partial r} + \frac{\partial u_z}{\partial z} = 0, \tag{5}$$

* By negative rotation we mean rotation in a sense opposite to the base flow direction.

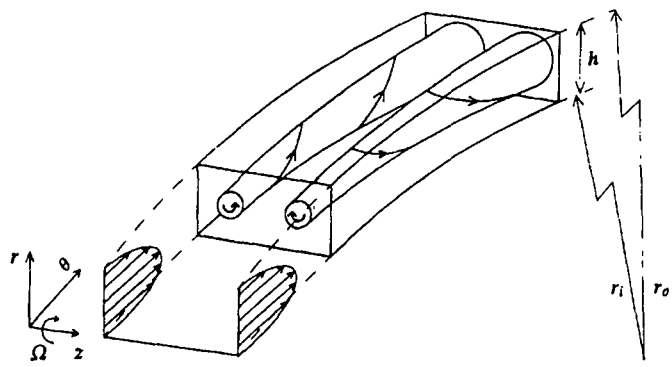

Figure 1. Sketch of problem

where

$$\frac{\mathrm{D}}{\mathrm{D}t} = \frac{\partial}{\partial t} + u_r \frac{\partial}{\partial r} + \frac{u_\theta}{r}\frac{\partial}{\partial \theta} + u_z \frac{\partial}{\partial z},$$

$$\nabla^2 = \frac{1}{r}\frac{\partial}{\partial r}\left(r\frac{\partial}{\partial r}\right) + \frac{1}{r^2}\frac{\partial^2}{\partial \theta^2} + \frac{\partial^2}{\partial z^2},$$

(u_r, u_θ, u_z) are the velocity components along r, θ and z respectively and p is the dimensionless pressure. The scalings used are the channel height h (equal to the difference between outer and inner radius, $r_o - r_i$) for length, the bulk speed U for velocity, h/U for time and ρU^2 for pressure, where ρ is the fluid density. The ensuing governing parameters are the Reynolds number and the rotation number,

$$Re = Uh/\nu, \qquad Ro = \Omega h/U, \tag{6}$$

with ν the kinematic viscosity.

The numerical method is the same as that used by Bottaro *et al.*[15] and Bottaro[6] to study the spatial development of Dean vortices. The main characteristics of the numerical technique follows. A finite volume staggered grid is constructed to cover the computational domain which is swept by zebra relaxation sweeps along radial and aximuthal directions. Convective and diffusive fluxes are treated with second-order centred schemes and the Thomas algorithm is used to solve the resulting tridiagonal system of equations. Steady solutions are obtained via fully implicit Euler time stepping; the time step $\mathrm{d}t$ is taken equal to 0·1 and is such that more than four steps are needed to advance a typical fluid element moving at the bulk speed of one streamwise mesh length. The pressure coupling is dealt with by the pressure correction technique SIMPLER described in detail by Patankar.[16] The computational domain extends from $z = 0$ to $z = z_{max}$ with $z_{max} = 1{\cdot}5$ and the spanwise length is such that one vortex pair of wave number $\beta = 4{\cdot}2$ can be accommodated in the cross-section. This β is equal to the average value measured by Matsson and Alfredsson[3] and is close to critical for $Ro = 0$. In the radial direction the domain goes from $r = r_i$ to r_o with $r_o - r_i = 1$ and $r_i = 37{\cdot}6$ in order to match the set-up of Matsson and Alfredsson.[2,3,9] The angular extent is 1·745 rad. The grid consists of 48 equally sized control volumes along the spanwise direction and 24 stretched control volumes along the normal-to-the-wall direction; the stretching is such that near-wall details are finely resolved. With such a grid a typical vortex pair is resolved in the cross-section by 1152 control volumes; such a resolution is clearly adequate and exceeds the minimal resolution requirements established by Bottaro[6] (p. 636) for a comparable flow configuration. Along the streamwise direction 150 equally

spaced grid points are used. For the channel of streamwise length $(r_i + r_o)\theta/2 = 66{\cdot}49$ in the present simulations this resolution translates to more than two control volumes along the streamwise direction for every non-dimensional unit of length. The resolution is acceptable for this kind of flow prior to the onset of the secondary, wavy instability. However, when such an instability arises, streamwise travelling waves of length approximately equal to h occur so that more grid points in θ will be needed to adequately capture the phenomenon. No-slip Dirichlet boundary conditions are applied at the solid walls and the spanwise direction is taken periodic.

The open boundary conditions are crucial in a convectively unstable flow such as the present one.[17] For the Dean flow[6] it was found that a steady forcing at the inlet was required to 'drive' the vortex development and to overcome the unsteady effects caused by the propagation of pressure waves between inlet and outlet boundaries. These effects were found to be responsible for states with continuous and seemingly random interactions—mergings and splittings—of vortices. These interactions produced *defects* with soliton-like behaviour. Although this subject is worthy of further investigations, the focus is on the primary, steady instability of the vortices.

The flow field imposed at the inlet of the domain consists of the exact, one-dimensional solution for curved channel flow, the expression of which is

$$U(r) = A(r \ln r + Cr + E/r), \tag{7}$$

with

$$A = -\frac{2}{(r_i + r_o)/2 + 2E \ln(r_i/r_o)(r_o - r_i)}, \quad C = \frac{r_i^2 \ln r_i - r_o^2 \ln r_o}{r_o^2 - r_i^2}, \quad E = -\frac{r_i^2 r_o^2}{r_o^2 - r_i^2} \ln\left(\frac{r_i}{r_o}\right), \tag{8}$$

plus a small perturbation which is taken to be

$$u_r' = -\epsilon \sin\left(\frac{r - r_i}{r_o - r_i}\pi\right) \cos(\beta z + \pi), \tag{9}$$

$$u_\theta' = 0, \tag{10}$$

$$u_z' = -\epsilon\left[\frac{1}{r\beta} \sin\left(\frac{r - r_i}{r_o - r_i}\pi\right) \sin(\beta z + \pi) - \frac{1}{\beta(r_o - r_i)} \pi \cos\left(\frac{r - r_i}{r_o - r_i}\pi\right) \sin(\beta z + \pi)\right], \tag{11}$$

with no-slip conditions explicitly enforced on the solid walls and with ϵ, the amplitude of the inlet disturbance, small: $\epsilon = 0{\cdot}01$. The perturbation chosen satisfies the continuity equation and represents a pair of vortices (see Fig. 2). Equation (9)–(11) are not the eigensolutions of the linear stability problem but constitute physically sound inlet conditions with a non-zero projection on the linear eigenfunction space. The numerical simulations performed show that Dean vortices start growing immediately from the proposed initial disturbance field.

The outlet conditions are expressed via *convective* derivatives of the form

$$\frac{\partial \psi}{\partial t} + U \frac{\partial \psi}{\partial x} = 0, \tag{12}$$

where ψ denotes each velocity component. Such conditions were found to produce negligible reflection of outgoing waves in a complex mixed convection problem (the Poiseuille–Bénard configuration[18]) which, at periodic time intervals, presented macroscopic regions of flow reversal at the exit boundary.

A note is in order concerning the advantage of simulations that use the *spatial* as opposed to the *temporal* model. A detailed discussion of the subject is given by Bottaro;[6] here it suffices to say that temporally developing simulations (i.e. those simulations that employ streamwise periodic

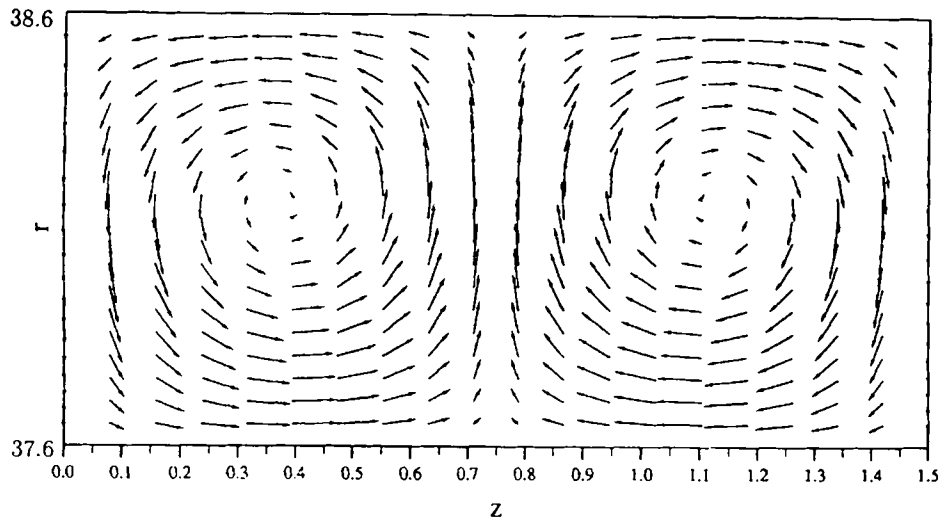

Figure 2. Initial condition

boundaries and that try to match spatial and temporal developments through the adoption of an *ad hoc* convection speed) may produce spurious, periodic time oscillations, resulting from the continuous creation and annihilation, in the computational cross-section, of a vortex pair. On the other hand, experiments carried out under conditions of steady inlet forcing[2,3,9] suggest that stationary and spatially developing vortex interaction phenomena occur.

3. RESULTS AND DISCUSSION

To illustrate the effect of system rotation on the vortices, we focus on the case of $Re = 432$ (the corresponding Dean number, defined as $De = Re\gamma^{0.5}$ with the curvature parameter γ given by $\gamma = 2(r_o - r_i)/(r_o + r_i)$, is equal to 70) and four different rotation numbers: $Ro = 0{\cdot}03, 0, -0{\cdot}03, -0.05$.

Before presenting the non-linear results, it is interesting to comment on the expected behaviour of the different flow cases by inspecting the generalized Rayleigh discriminant. The flow is inviscidly unstable to axisymmetric perturbations in regions where Φ is negative. From Figure 3 one would expect the instability to arise near the concave wall for $Ro = 0$ and 0·03 and near the convex wall for $Ro = -0{\cdot}05$. When $Ro = -0{\cdot}03$, four alternating regions of positive and negative Φ are present across the radial direction and this is interpreted as an indication that some global balance between Coriolis and centrifugal effects occurs. The linear stability theory[9] confirms that the flow is stable up to large values of Re when Ro is in the neighbourhood of $-0{\cdot}03$.

Results for the reference case $Ro = 0$ are displayed in Figure 4 from the top in terms of streamwise perturbation velocity isolines and secondary flow vectors on several cross-sections* and of streamwise perturbation energy as a function of θ. The open circles in the last figure are the results by Matsson and Alfredson.[3] The streamwise perturbation velocity is defined as

$$u'(r, \theta, z) = u_\theta(r, \theta, z) - \bar{u}(r, \theta), \quad \text{where } \bar{u}(r, \theta) = \frac{1}{z_{max}} \int_0^{z_{max}} u_\theta(r, \theta, z)\mathrm{d}z, \tag{13}$$

* Note that the curved channel has been 'straightened' for graphical purposes.

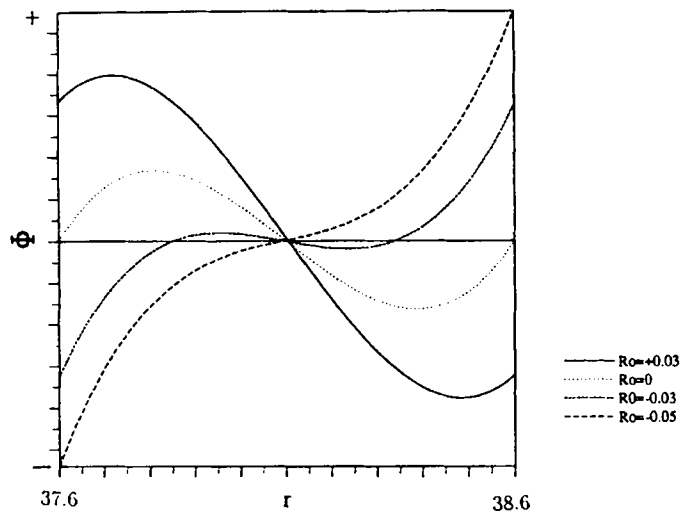

Figure 3. Generalized Rayleigh discriminant for various rotation numbers

and the corresponding disturbance energy is

$$e = \sqrt{\left(\frac{1}{A}\int_A (u')^2 \mathrm{d}A\right)}, \tag{14}$$

with A the cross-sectional area.

The agreement between the computed and the measured perturbation energies is very good, although the experimental results present a higher background disturbance level that shows up to θ of about 0·6. The computed e grows exponentially from $\theta = 0$ rad up to $\theta \approx 1$ rad. At that point, non-linear effects become predominant and after an overshoot a saturation characterized by a quasi-parallel pair of vortices appears. The details of the streamwise perturbation velocity on several cross-sections are well captured by the simulation as attested by a comparison between Figure 4 (top) and Figure 5(a). In Figure 5 we have reported the hot wire results of Matsson and Alfredsson[3] for u' at three cross-sections in the non-linear regime separated by an angular distance of 0·787 rad from one another. An elongated (along z) high-speed region is formed near the concave wall for $Ro = 0$ and it is delimited by two thin, vigorous upwash zones with secondary flows from the outer to the inner surface.

The picture is completely modified when a small negative rotation is applied. Figure 6 shows that the perturbation energy in both the experiment and the computation at $Ro = -0{\cdot}03$ does not grow from its background level and vortices do not form in the allotted streamwise distance. Conversely, by decreasing Ro further ($Ro = -0{\cdot}05$), a pair of cells starts to emerge in the Coriolis-unstable region close to the convex wall (Figure 7). The computational domain is not long enough in θ to allow for a full amplification of the instability; however, the experimental results in Figure 5(b) demonstrate that the vortices become just like those of the $Ro = 0$ case, with the roles of concave and convex walls reversed (the flow structures are 'upside-down').

For the positive rotation case ($Ro = 0{\cdot}03$) a rapid growth of e is found with a peak for θ as low as 0·8 rad (Figure 8). The large amplification factor of the instability is due to the combined effect of centrifugal and Coriolis forces. An interesting phenomenon occurs from $\theta \approx 1{\cdot}1$ rad: the elongated

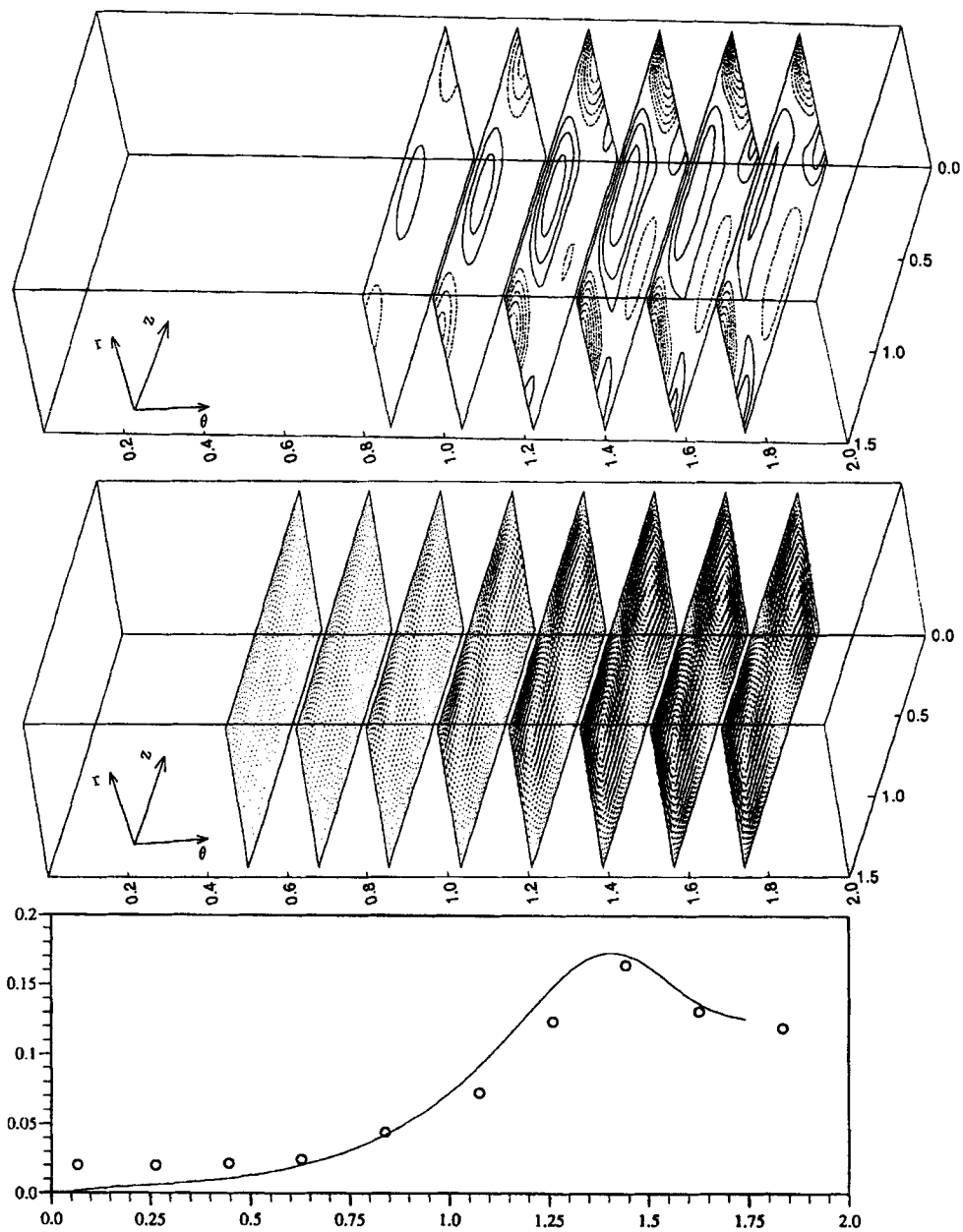

Figure 4. $Ro = 0$. From the top, isolines of streamwise perturbation velocity (contour increment, scaled with U, is 0·075, negative contours are shown with broken lines and the zero lines are omitted), secondary flow velocity vectors and streamwise disturbance energy (e versus θ) are shown. The open circles are the experimental results of Matsson and Alfredsson[3]

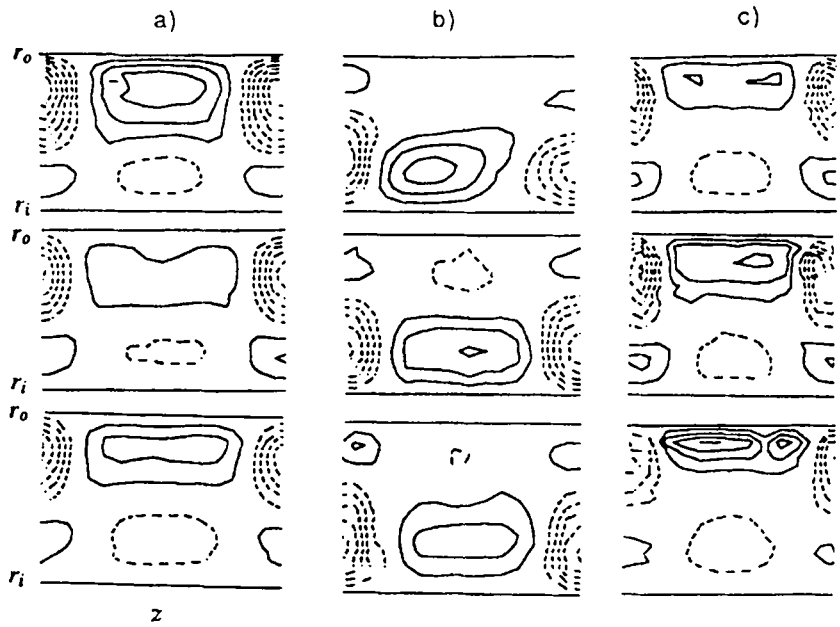

Figure 5. Experimental results by Matsson and Alfredsson[3] for streamwise perturbation energy, with same isoline spacings as Figure 4: (a) $Ro = 0$; (b) $Ro = -0{\cdot}05$; (c) $Ro = 0{\cdot}03$. The three streamwise stations shown at each rotation number are separated by an angular distance of 0·787 rad from one another

high-velocity region by the concave wall splits into two smaller regions with a small, negative u' cell in between. This marks the beginning of a splitting event and a new state starts forming with twice the wave number of the input condition. This effect of positive system rotation is not unexpected, since both the experiments of Matsson and Alfredsson[3] and work on rotating flat plate boundary layers[19] indicate that the number of naturally appearing vortices increases under conditions of positive rotation.

To further attest to this fact, another computation was conducted in a longer (along z) domain. The purpose of this was to facilitate the appearance and rapid growth of a new vortex pair via a generalized Eckhaus instability. For the value of the spanwise wave number of this last calculation ($\beta = 2{\cdot}51$) the linear theory predicts a slower growth than in the previous case. This is confirmed by

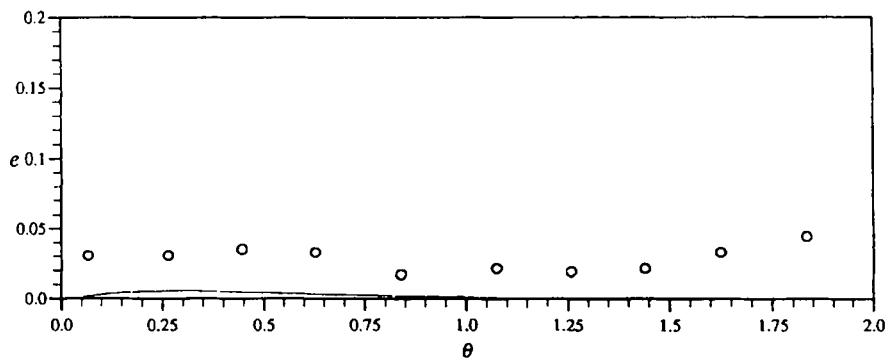

Figure 6. Streamwise disturbance energy for $Ro = -0{\cdot}03$

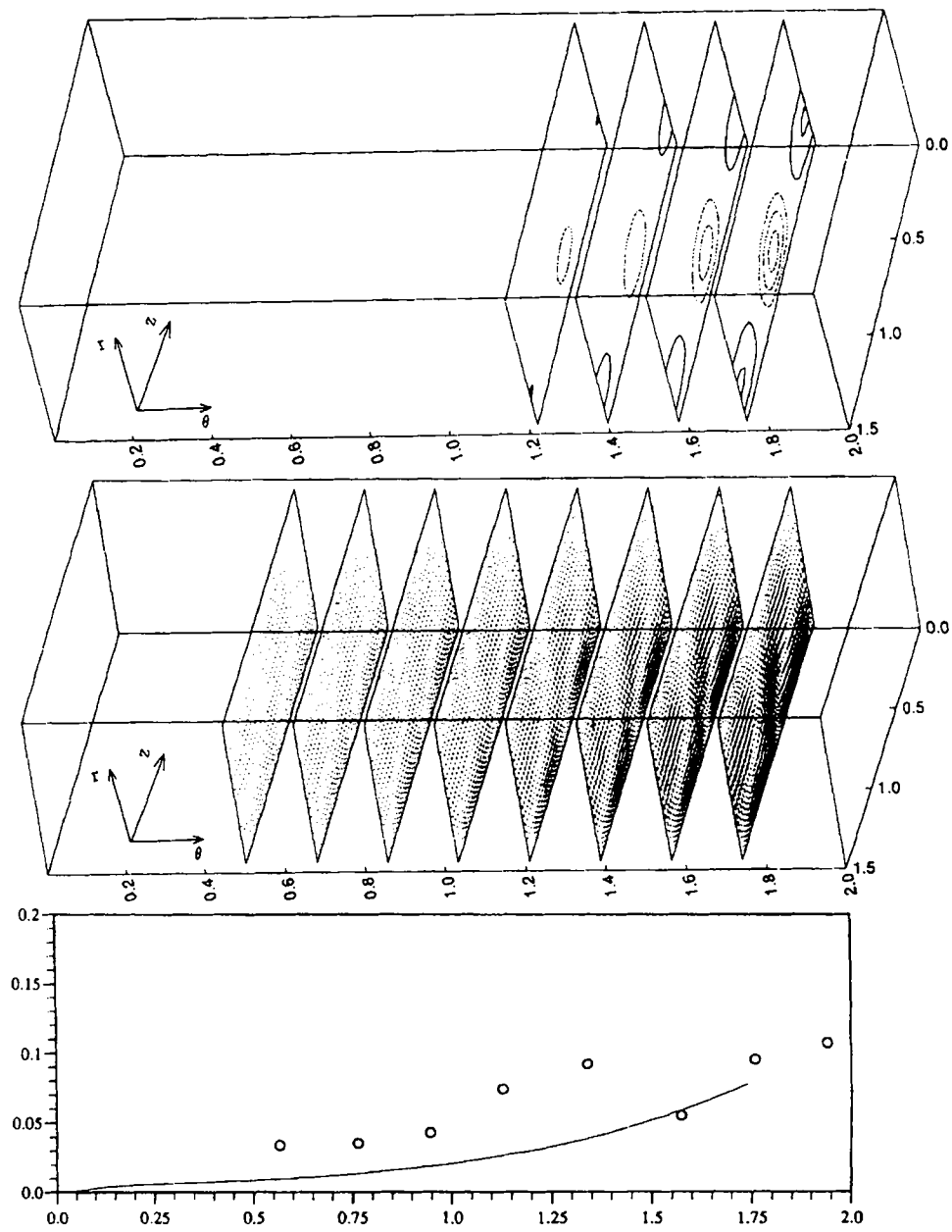

Figure 7. Same as Figure 4 but for $Ro = -0{\cdot}05$

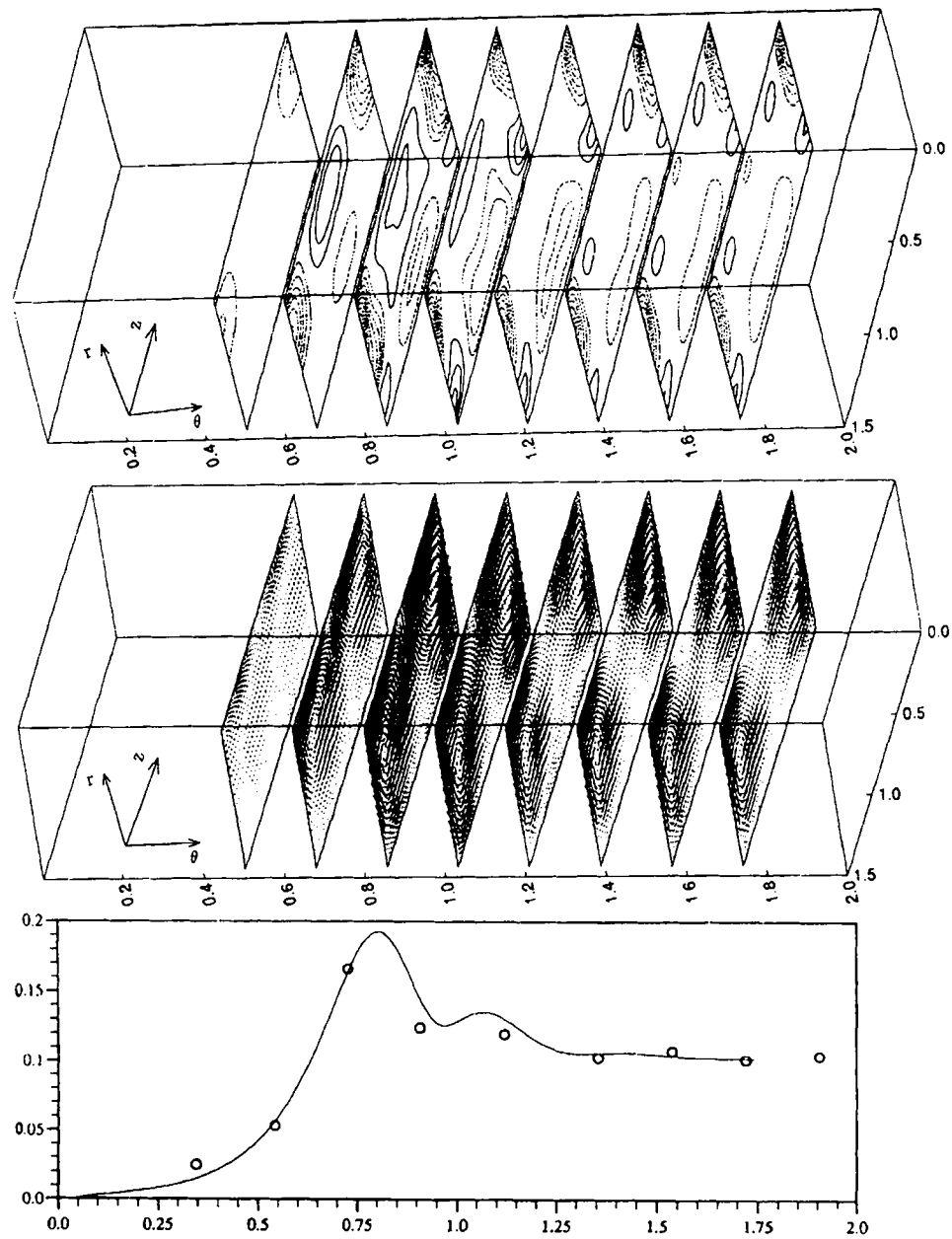

Figure 8. Same as Figure 4 but for $Ro = 0{\cdot}03$

the calculation (Figure 9). The perturbation energy peak is reached at $\theta = 0{\cdot}87$ and such a maximum value is slightly inferior to that attained by vortices with $\beta = 4{\cdot}2$. Starting from $\theta \approx 1{\cdot}0$, a new vortex pair starts appearing at the concave wall midway between $z = 0$ and z_{max}. This new structure, clearly evidenced by plots of both the streamwise disturbance velocity and the secondary flow, rapidly acquires strength and produces a second, well-marked overshoot in e close to the exit of the computational domain. The final, stable flow configuration at the channel exit consists of two pairs of counter-rotating vortices, although only one pair was forced at the inlet.

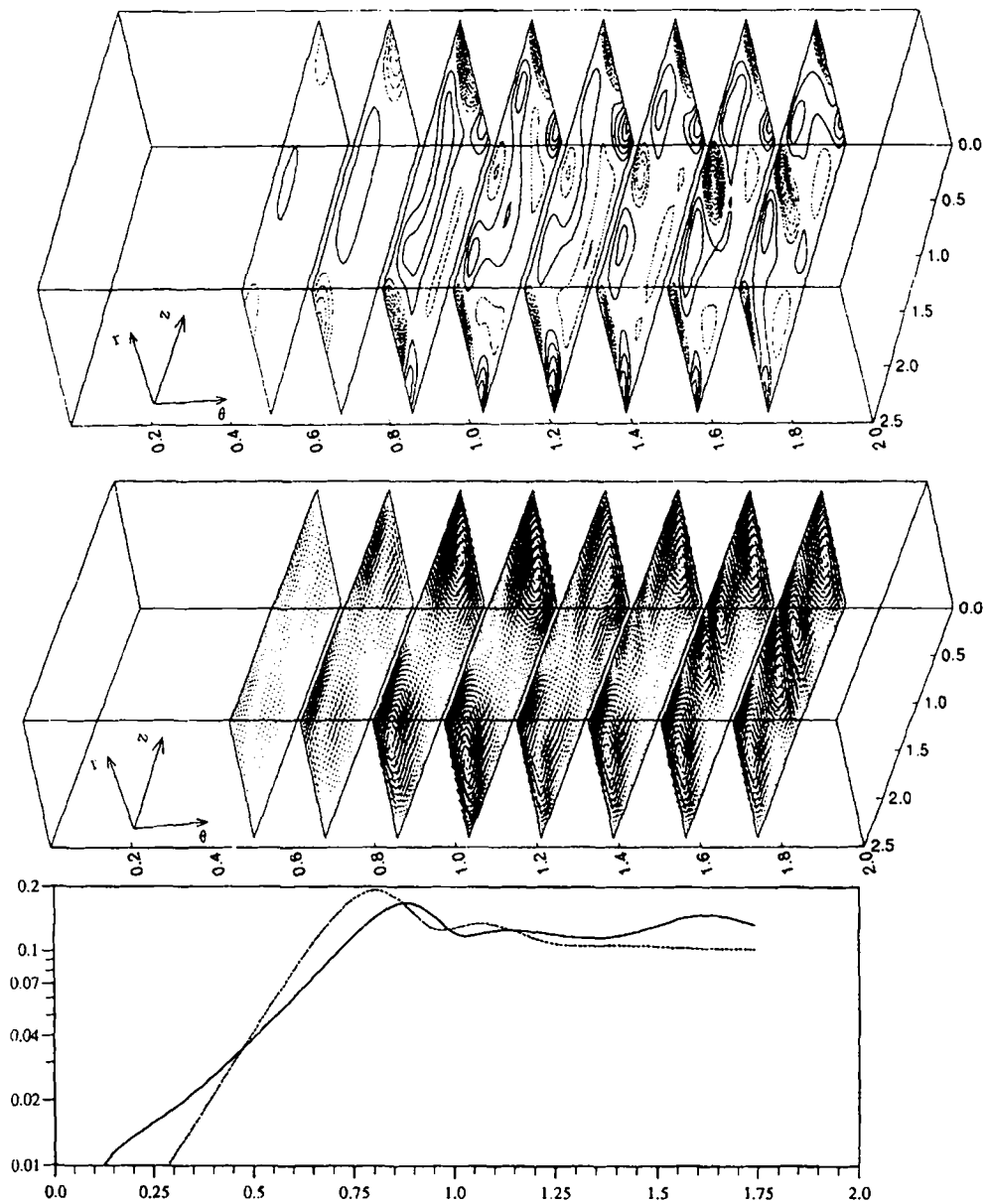

Figure 9. Same as Figure 8 for $\beta = 2{\cdot}51$. The broken curve in the e versus θ plot is the result for $\beta = 4{\cdot}2$

The difference between the case with $\beta = 4{\cdot}2$ and that with $\beta = 2{\cdot}51$ can also be nicely illustrated by isosurface plots of the streamwise vorticity. In Plate 1(a) the initial formation of a second vortex pair is not visible (this is, however, due to the values of the streamwise vorticity chosen for the graphical representation). In contrast, in Plate 1(b) a suggestive structural bifurcation appears whereby from the large-scale regions of positive and negative vorticity near the outer wall, two symmetric 'legs' emerge that tend to invade the centre of the cross-section. These two legs in turn induce, a bit further downstream, opposite sign vorticity at the concave wall in such a way that at the channel outlet two quasi-fully developed pairs of streamwise vortices appear.

4. CONCLUDING REMARKS

In this work, three-dimensional, spatially developing Navier–Stokes calculations have been described for the rotating Dean flow case. It has been shown that depending on the rate of rotation of the system, different instabilities (Coriolis-dominated or centrifugally dominated) may arise with amplification rates that can range from very large to negligibly small. Extensive comparisons with experimental data have been made to attest the validity of the simulations.

Convincing evidence for the appearance of a generalized Eckhaus instability has been presented for the positive rotation case. This may warrant further theories for secondary, non-linear instabilities of rotating vortices.

ACKNOWLEDGEMENTS

The financial support from the Swiss National Fund, grant 21-40467.94, and the computing time on the Cray YM-P provided by the Service Informatique Centrale of EPFL are gratefully acknowledged. We wish to thank Professor I. L. Ryhming for helpful discussions on the subject of this work.

REFERENCES

1. W. R. Dean, 'Fluid motion in curved channel', *Proc. R. Soc. Lond. A*, **128**, 402 (1928).
2. O. J. E. Matsson and P. H. Alfredsson, 'Experiments on instabilities in channel flow', *Phys. Fluids A*, **4**, 1666 (1992).
3. O. J. E. Matsson and P. H. Alfredsson, 'The effect of spanwise system rotation on Dean vortices', *J. Fluid Mech.*, **274**, 243 (1994).
4. P. M. Ligrani, J. E. Longest, M. R. Kendall and W. A. Fields, 'Splitting, merging and spanwise wavenumber selection of Dean vortices', *Exp. Fluids*, **18**, 41 (1994).
5. W. H. Finlay, J. B. Keller and J. H. Ferziger, 'Instability and transition in curved channel flow', *J. Fluid Mech.*, **194**, 417 (1988).
6. A. Bottaro, 'On longitudinal vortices in curved channel flow', *J. Fluid Mech.*, **251**, 627 (1993).
7. G. Guo and W. H. Finlay, 'Wavenumber selection and irregularity of spatially developing Dean and Görtler vortices', *J. Fluid Mech.*, **264**, 1 (1994).
8. Y. Guo and W. H. Finlay, 'Splitting, merging and wavelength selection of vortices in curved and/or rotating channel flow due to the Eckhaus instability', *J. Fluid Mech.*, **228**, 661 (1991).
9. O. J. E. Matsson and P. H. Alfredsson, 'Curvature and rotation-induced instabilities in channel flow', *J. Fluid Mech.*, **210**, 537 (1990).
10. O. J. E. Matsson, 'Time-dependent instabilities in curved rotating channel flow', *Phys. Fluids A*, **5**, 1514 (1993).
11. I. Mutabazi, C. Normand and J. E. Wesfreid, 'Gap size effects on centrifugally and rotationally driven instabilities', *Phys. Fluids A*, **4**, 1199 (1992).
12. A. Aouidef, J. E. Wesfreid and I. Mutabazi, 'Coriolis effects on Görtler vortices in the boundary layer flow on concave wall', *AIAA J.*, **30**, 2779 (1992).
13. A. Zebib and A. Bottaro, 'Görtler vortices with system rotation: linear theory', *Phys. Fluids A*, **5**, 1206 (1993).

14. A. Bottaro, B. G. B. Klingmann and A. Zebib, 'Görtler vortices with system rotation', *Theor. Comput. Fluid Mech.*, in press, 1996.
15. A. Bottaro, O. J. E. Matsson and P. H. Alfredsson, 'Numerical and experimental results for developing curved channel flow', *Phys. Fluids A*, **3**, 1473 (1991).
16. S. V. Patankar, *Numerical Heat Transfer and Fluid Flow*, McGraw-Hill, New York, 1980.
17. P. Huerre and P. A. Monkewitz, 'Local and global instabilities in spatially developing flows', *Ann. Rev. Fluid Mech.*, **22**, 473 (1990).
18. A. Bottaro, 'Note on open boundary conditions for elliptic flows', *Numer. Heat Transfer B*, **18**, 243 (1990).
19. M. Matsubara and S. Masuda, 'Three dimensional instability in rotating boundary layer', in D. C. Reda, H. L. Reed and R. Kobayashi (eds), *Boundary Layer Stability and Transition to Turbulence*, ASME, FED Vol. 114, 1991, p. 103.

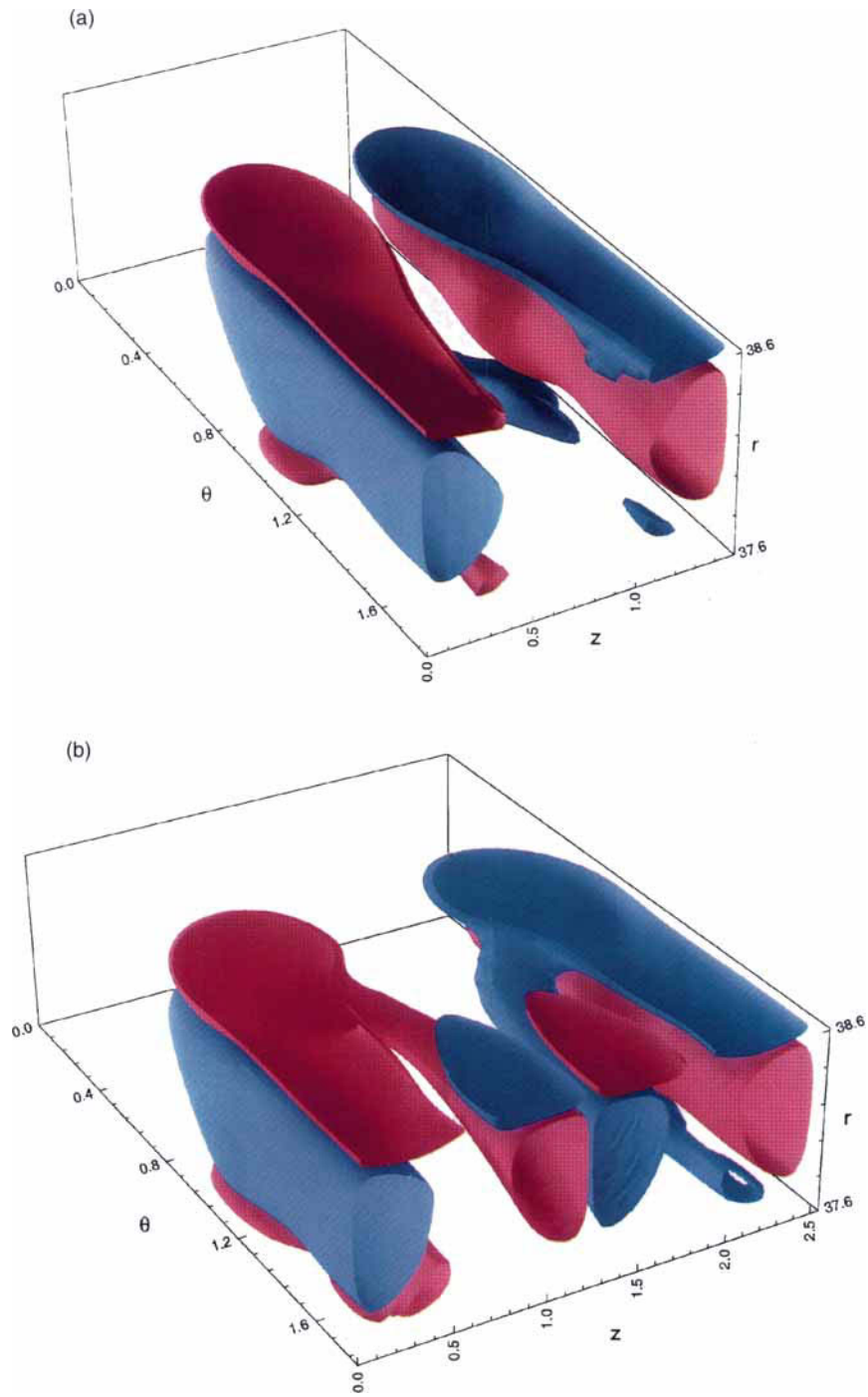

Plate 1. Isosurfaces of streamwise vorticity for Ro=0·03 with (a) β=4·2 and (b) β=2·51. The two values chosen for the display are +0·2 (blue) and –0·2 (red). The extrema of the streamwise vorticity are (a) 1·41 and (b) 2·1